NUCLEAR INSTRUMENTS AND METHODS 114 (1974) 417–423; © NORTH-HOLLAND PUBLISHING CO.

A MECHANICAL TIME-OF-FLIGHT NEUTRON DIFFRACTOMETER*

J. M. CARPENTER, D. F. R. MILDNER, C. A. PELIZZARI, J. D. SUTTON and J. E. GUNNING

Department of Nuclear Engineering, The University of Michigan, Ann Arbor, Michigan 48105, U.S.A.

Received 10 July 1973

A mechanical time-of-flight (TOF) neutron diffractometer has been constructed and a system of data analysis developed for the study of noncrystalline substances through radial density functions. Measurements to wave vector transfer $Q_{max} > 25$ Å^{-1} are readily made; a resolution $\Delta Q/Q < 2\%$ is obtained over most of the wave vector transfer range. Radial density functions computed using data from this instrument have a spatial resolution $\Delta r \approx 2\pi/Q_{max} \approx 0.25$ Å. These can be partially corrected for termination errors to provide a spatial resolution $\Delta r < 0.15$ Å.

1. Introduction

In studies of the structure of noncrystalline substances, diffraction measurements are used to determine the radial density function (rdf). This function is related to the static structure factor via a simple Fourier transform according to the Zernicke–Prins[1]) relation. Various limitations attend the choice of a particular diffraction technique. X-ray measurements give the static structure factor nearly rigorously and with high resolution, but suffer problems in removal of Compton scattered radiation, compensation for the varying atomic scattering factors and substantial absorption in the sample. Neutron measurements may easily be extended over larger wave vector transfer ranges, and the availability of isotopic substitution techniques is appealing; however there are inelastic scattering contributions which may invalidate the

* Work supported in part by National Science Foundation grant number GK-35901.

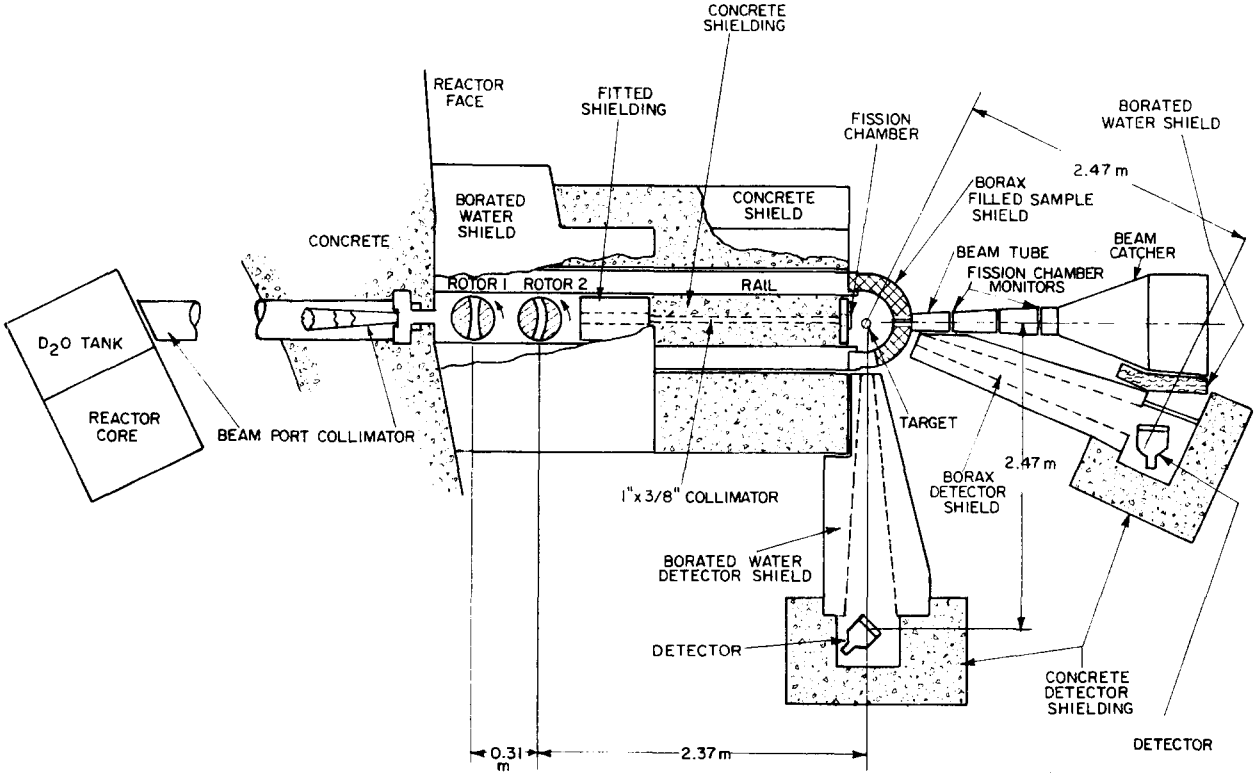

Fig. 1. Schematic drawing of the two-rotor time-of-flight diffractometer.

static approximation, as well as substantial absorption and multiple scattering. Electron diffraction is limited by applicability only to thin samples and surfaces.

The present work describes the TOF diffractometer recently constructed at the University of Michigan's Ford Nuclear Reactor. The design incorporates a configuration with equal flight paths before and after scattering, with which the static approximation is made most nearly valid[2]). Two rings of detectors are arranged in time-focused geometry[3]). Use of neutrons with energies up to nearly 1 eV provides a very large range of wave vector transfer, thus improving the quality of rdf's computed from these data. A vanadium reference method is used to account for variations in incident flux and detector efficiency.

2. General description

As shown in fig. 1, the diffractometer operates at beam port J of the 2 MW Ford Nuclear Reactor, viewing the D_2O source tank[4]). Thermal flux at the source is 2×10^{13} n/cm^{2}s. The neutron beam is coarsely collimated before passing through two rotors: first a fiberglass-resin rotating collimator, and second a curved-slit chopping rotor of Nimonic-90, a nickel alloy (see below). Scattered intensities measured by neutron scintillation detectors in banks at scattering angles of 20° and 90° are time analyzed by a TMC 1024 channel TOF analyzer, and the IBM 360/67 computer at the University's Computing Center is used to correct and transform the raw data to final rdf form.

3. Collimation

The neutron beam is defined by a 103″ long beam port plug. (This replaces the previous beam port plug which was similarly constructed but slightly shorter in length. However, it had much greater angular divergence caused by larger entrance and exit dimensions. All data shown in this paper used this earlier plug. Data taken with the new plug installed show that the background has been reduced considerably.) It has a vertical angular divergence of 0.0319 rad and a horizontal angular divergence of 0.0091 rad. The entrance slit dimensions are 4.61″ (vertical) × 33″ (horizontal) and the exit, 1.97″ × 0.54″. The plug is composed of alternate sections of graphite, concrete and lead, housed in a $7\frac{1}{2}$″ diameter aluminum tube.

Collimation between the chopper and target consists of a 95″ long rectangular aperture of dimensions 1″ (vertical) × $\frac{3}{8}$″ (horizontal). Together with the 1″ × $\frac{1}{4}$″ chopper rotor, this aperture defines a collimating system of angular divergence 0.0092 rad (vertical) × 0.0079 rad (horizontal). The beam size at the target position is thus $1\frac{1}{2}$″ × $\frac{1}{2}$″.

4. Spinning heads and associated electronics

The rotors are driven and supported by spinning heads of the Harwell type[5]). Each contains windings for a three-phase hysteresis synchronous drive motor which can be rotated about the shaft axis for rotor phasing adjustments. A dc lifting magnet suspends the shaft-rotor assembly as it turns in air journal bearings. Each rotor spins in a 2″ thick steel housing evacuated to approximately 10 μm Hg. The 0.188″ diameter wire from which the rotor hangs, extends through an oil-filled damper assembly which serves both to inhibit rotor oscillations and seal the vacuum chamber.

Driving power is provided as shown schematically in fig. 2. The signal generator drives the amplifiers at any of 13 frequencies from 140 to 480 Hz controlled by a precision tuning-fork oscillator (the rotating collimator is driven at half the basic frequency). In practice, measurements are made at only two or three different rotor speeds. A variable time delay between the openings of rotors 1 and 2 is adjusted by rotating the stator of one drive motor about its shaft in the appropriate sense. Timing signals are derived through a magnetic pickup from an iron slug in a 1.5″ diameter aluminum disk mounted on each motor shaft. These signals start and stop a 1-MHz gated clock. A trigger signal is generated after a variable delay of 1 to 2047 μs after the opening of rotor 2, and is used to start the analyzer counting cycle on each rotor revolution.

5. Detection systems

Neutron detectors are mounted in banks at scattering angles of 20° and 90°. The 20° bank of four detectors subtends an azimuthal angle of 14.7° and solid angle of

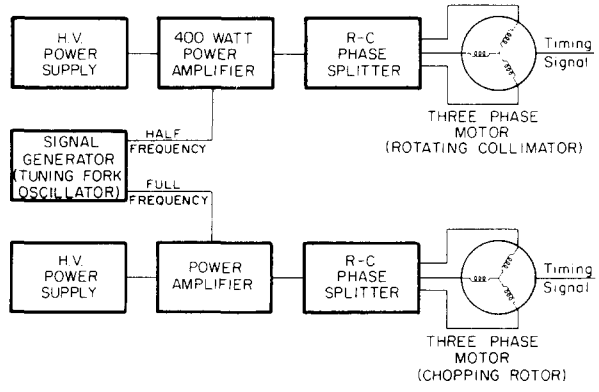

Fig. 2. Rotor driving power system block diagram.

3×10^{-3} sr, and the 90° bank of seven detectors subtends an azimuthal angle of 27.8° and solid angle of 1.5×10^{-2} sr. Each detector unit consists of a scintillator plate, light guide, photomultiplier tube, voltage divider and emitter-follower output circuit. The scintillators are of the Stedman type[6]), one part by weight ^{6}LiF and two parts ZnS(Ag) bound with one part polymethyl methacrylate (PMMA) plastic. The three powders are mixed and hot-pressed into $5'' \times 5''$ sheets.

For the detectors used at 90°, 1 mm (0.19 g/cm^2) thick plates were corrugated and molded to matching PMMA backing plates approximately 3 mm thick; these were bonded with optical epoxy cement to boron glass (Vycor) plates. For the 20° detectors, 0.045 g/cm^2 flat scintillator plates were bonded directly to Vycor plates using optical epoxy cement.

The Vycor plates are coupled to PMMA light guides using optical grease (Dow–Corning 120-057). A similar joint is made between the light guides and 5″ diameter (Dumont 6364) photomultiplier tubes. Each tube has a potted voltage divider to which are added dropping resistors for matching of units, as well as an emitter follower.

Detector signals are fed through individual pulse shape discriminators[7,8]) for elimination of gamma pulses and background noise. Discriminated signals are routed through or-gates and via the four-input "Quadapter" (described below) to the TOF analyzer.

6. Time-of-flight analysis

The Technical Measurements Corporation model CN-1024 multichannel analyzer with slightly modified model 212 time-of-flight logic unit provides 1024 time channels of width from $\frac{1}{4}$ to 192 μs, capacity $2^{17}-1$ per channel. The variable delay trigger described above begins the analysis after each opening of the chopping rotor. Normally four scattered intensity distributions are analyzed in 256 channel memory segments: sample scatterer at large and small angles, and reference scatterer at each angle. Backgrounds (primarily due to fast neutrons) are either measured separately or interpolated between regions of no sample signal. The Quadapter[9]) is used in conjunction with a sample cycler to route data from the large and small angle detector banks to appropriate sections of the analyzer memory, and to alternate sample with reference counting. Alternation of the sample and reference scatterers for counting periods of several minutes eliminates concern over long-term fluctuations in reactor power, possible minor temperature-dependent drifts in detector efficiency, and fluctuations in the inter-rotor phasing.

7. Vanadium reference method

In the static approximation, the result of a TOF diffraction measurement can be expressed in the form

$$C(t,\theta) = N_0 T_{\mathrm{eff}} A_{\mathrm{b}} \Delta\Omega \phi(E) F(E,\theta) \eta(E) \times \times J(E,t) \Delta t \frac{\mathrm{d}\sigma(Q)}{\mathrm{d}\Omega},$$

where

$$Q = 2k \sin \tfrac{1}{2}\theta, \quad k + m_{\mathrm{n}} v/\hbar, \quad v = L/t,$$

$C(t, \theta)$ = observed counting rate at neutron time of arrival t, for a detector at angle θ,
L = total flight path length (incident + scattered),
N_0 = number of scattering units per unit volume in the target,
T_{eff} = effective thickness of the target along the incident beam direction,
A_{b} = incident beam area,
$\Delta\Omega$ = solid angle subtended by the detector at the target,
$\phi(E)$ = incident neutron flux per unit energy at energy E,
$F(E, \theta)$ = correction factor accounting for effects of attenuation and multiple scattering,
$\eta(E)$ = detector efficiency for neutrons of energy E,
Δt = the analysis channel width, i.e., the time window at time t,
$J(E, t)$ = $\partial E/\partial t = 2E/t$,
$\mathrm{d}\sigma(Q)/\mathrm{d}\Omega$ = the differential cross section associated with wave vector transfer Q.

In principle, all of the factors in the above equation can be measured or calculated. In practice however, it is simpler to perform a similar measurement with a reference scatterer of known cross section and to form the ratio

$$\frac{C^{\mathrm{S}}(t,\theta)}{C^{\mathrm{R}}(t,\theta)} = \frac{N_0^{\mathrm{S}} T_{\mathrm{eff}}^{\mathrm{S}} A_{\mathrm{b}} \Delta\Omega \phi^{\mathrm{S}}(E) F^{\mathrm{S}}(E,\theta) \eta^{\mathrm{S}}(E) J(E,t) \Delta t \, \mathrm{d}\sigma^{\mathrm{S}}(Q)/\mathrm{d}\Omega}{N_0^{\mathrm{R}} T_{\mathrm{eff}}^{\mathrm{R}} A_{\mathrm{b}} \Delta\Omega \phi^{\mathrm{R}}(E) F^{\mathrm{R}}(E,\theta) \eta^{\mathrm{R}}(E) J(E,t) \Delta t \, \mathrm{d}\sigma^{\mathrm{R}}(Q)/\mathrm{d}\Omega}.$$

If the sample and reference scatterers are alternated in the scattering position for short intervals (several minutes), then on average, $\phi^{\mathrm{S}}(t) = \phi^{\mathrm{R}}(t)$ and $\eta^{\mathrm{S}}(t) = \eta^{\mathrm{R}}(t)$, as it is expected that any variations in incident neutron spectrum or detector efficiency will be unimportant over the period of target alternation. In practice,

variations are both small and of long term. The sample differential cross section is then

$$\frac{d\sigma^S(Q)}{d\Omega} = \frac{C^S(t,\theta)}{C^R(t,\theta)} \frac{N_0^R T_{eff}^R F^R(E,\theta)}{N_0^S T_{eff}^S F^S(E,\theta)} \frac{d\sigma^R(Q)}{d\Omega}.$$

The reference scatterer used is a vanadium metal slab of dimensions $4'' \times 2'' \times 0.125''$, density 0.0720 atoms/b cm. The coherent and incoherent scattering cross sections of vanadium are 0.034 and 5.13 b[10]) and scattering from vanadium is predominantly elastic; this choice of reference scatterer particularly simplifies data analysis, since $d\sigma^R/d\Omega = 5.13/4\pi$ b/sr, and constant[11]) to excellent approximation. [Since vanadium has been so frequently used as a reference scatterer and since an uncertainty of several percent remains in the value of the vanadium incoherent scattering cross section, we would recommend a new determination of its value, as has earlier been suggested by Page[12]).]

8. Instrumental range

The most significant advantage of the presently described instrument is its ability to obtain diffraction data over a very wide range of wave vector transfer Q with good resolution and intensity. Most important is the extension of the range to the region beyond 20 $Å^{-1}$ which is accessible to X-ray measurements only through application of extreme measures[13]). A recent measurement of the diffraction pattern of vitreous BeF_2 shows the detail observable at large Q.

As seen from the wave vector transfer relation for elastic scattering $Q = 2k \sin \frac{1}{2}\theta$, for fixed scattering angle large wave vector transfers are reached using large incident neutrons wave numbers; i.e., high energy neutrons. For 90° scattering, 30 $Å^{-1}$ wave vector transfer requires neutron energy of 0.934 eV. The suitability of this instrument for measurements with such high energy neutrons is due to the properties of the slow-neutron chopping rotor[5]), which was obtained from the disassembled Chalk River Thermal Neutron Analyzer[14]). This rotor is constructed of Nimonic-90, the composition of which is given in table 1. The neutron cross section of this alloy is shown in fig. 3 along with the "chopping angle" α_c, defined as the additional angle through which the rotor must turn to introduce at least one mean-free-path thickness of material into all parts of the incident beam path, beyond that necessary for a rotor of perfectly opaque material. This admittedly idealized parameter gives an idea of the relative ability of the rotor to effectively chop

TABLE 1

Composition of Nimonic-90 alloy (from Metals Handbook, 1954 supplement; American Society for Metals, Cleveland, 1954).

Element	Weight %
Ni	58.0
Cr	20.0
Co	16.0
Ti	2.3
Al	1.4
Fe	0.5
Mn	0.5
Si	0.4
C	0.08

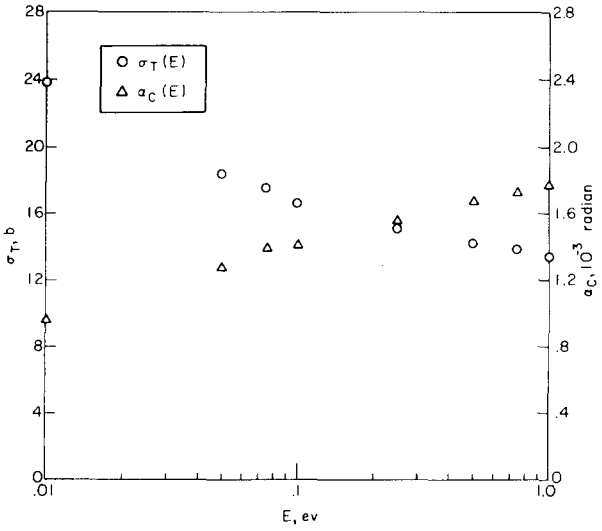

Fig. 3. Total neutron cross section σ_T and "chopping angle" α_c (defined in text) for Nimonic-90 alloy.

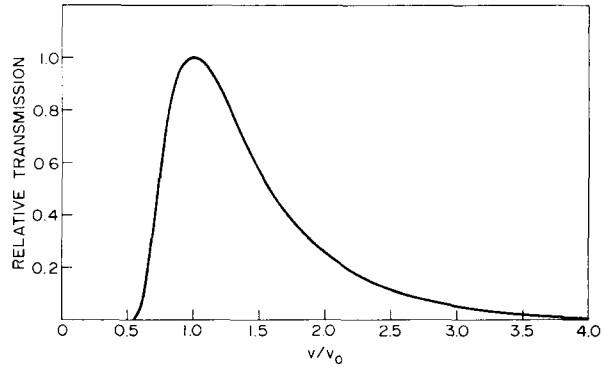

Fig. 4. Transmission function for a 10″ diameter rotor with a single ¼″ slit of circular arc centerline and 40″ radius of curvature.

a beam at the various energies; small values are clearly to be desired compared to the slit angular divergence, 0.025 rad. The rotor's performance does not appreciably diminish even at 1 eV; the time width of the chopper burst remains essentially equal to that for a rotor of opaque material. 1 eV is a much higher energy than is conventionally used in diffraction measurements (in fact, the fall-off of the reactor neutron spectrum at high energies is a more practical limitation than the instrumental ability to chop a high energy beam).

The 10″ diameter Nimonic-90 rotor is constructed with three $\frac{1}{4}$″ slits of circular-arc centerline, having a 40″ radius of curvature; the ratio of optimum transmitted velocity to rotor tip velocity is 16. Optimum transmission energies range from 0.016 eV at a rotor frequency of 140 Hz to 0.196 eV at 480 Hz. Energies considerably higher and lower than optimum are of course transmitted, as seen in fig. 4. The transmission function shown was calculated using the results of Stone and Slovacek[15]) with $1/V$ replaced everywhere by $|V^{-1} - V^{-1}|$, where $V_0 = 16R\omega = 2.032\ \omega$ (m/s) for the Nimonic rotor described here ($R = 5''$, ω = rotor angular frequency). This is the correct generalization of the straight-slit results of Stone and Slovacek to rotors with Archimedes' spiral or (approximately) circular slits[16]).

In practice, the lowest wave vector transfer for which good quality data are obtained is about 0.95 $Å^{-1}$ at 140 Hz and 20° scattering angle; the highest, about 27 $Å^{-1}$ at 480 Hz and 90°.

9. Resolution

Since a reasonable knowledge of the instrumental resolution function is necessary in the careful interpretation of diffraction data, much effort has been expended in both calculation and measurement of this function.

Three separate calculations have been made; the motivation for and result of each are here briefly described.

(1) Using a "time-focusing" method, two loci[3]) of optimum resolution for the diffractometer were calculated. The plane detectors (see above) were placed tangent to these loci at the 20° and 90° scattering angles, and detector rocking experiments verified that resolution broadening was indeed minimized at the predicted orientations even though the time focusing calculation ignores the detailed effects of the chopping rotor. The method gives no estimate of the actual resolution broadening, yielding only the optimum detector orientation.

2) A calculation of the time variance of the pulse

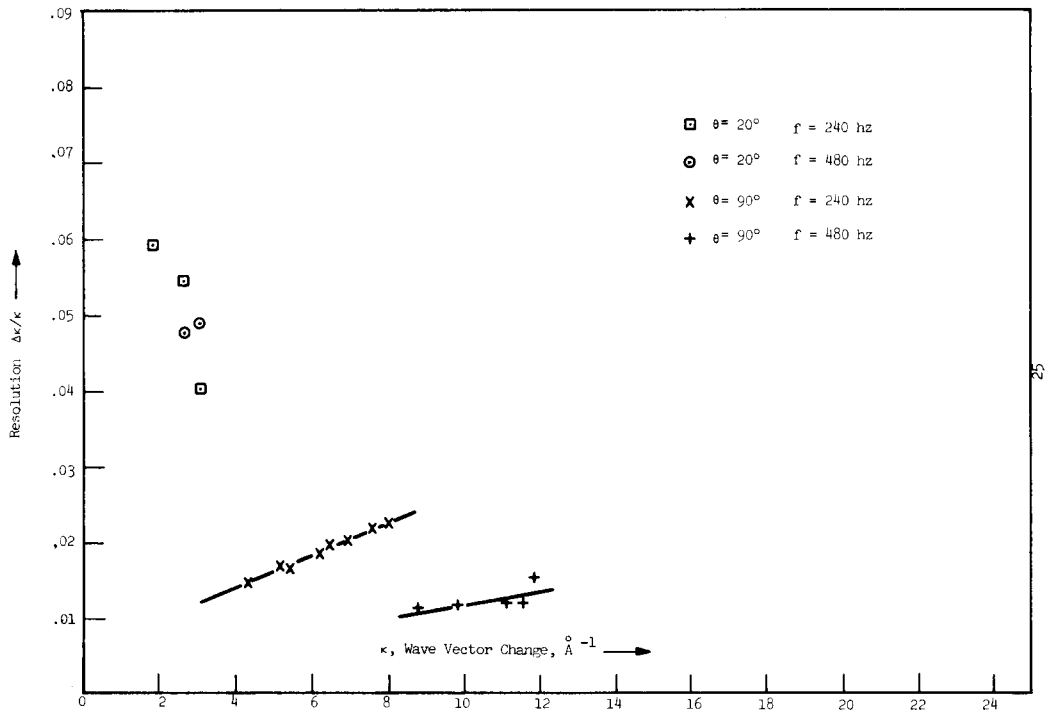

Fig. 5. Resolution characteristics of the time-of-flight diffractometer. Symbols represent measured width of polycrystal diffraction lines; solid lines represent calculated models described in text.

scattered from a single reciprocal lattice vector was made, treating the source (rotor) and detector as points and the target as an infinite plane. A realistic treatment of the time and angular variances and time–angle covariance of the rotor was included, derived from a geometrical treatment of the chopper burst shape.

3) An extension of (2) and (3) is summarized in fig. 5 together with resolution widths measured as described below. These calculations and measurements are used to account for resolution broadening in diffraction data. Expressions for the results of (2) and (3) are too lengthy to be repeated here.

Measurements of resolution widths were made using

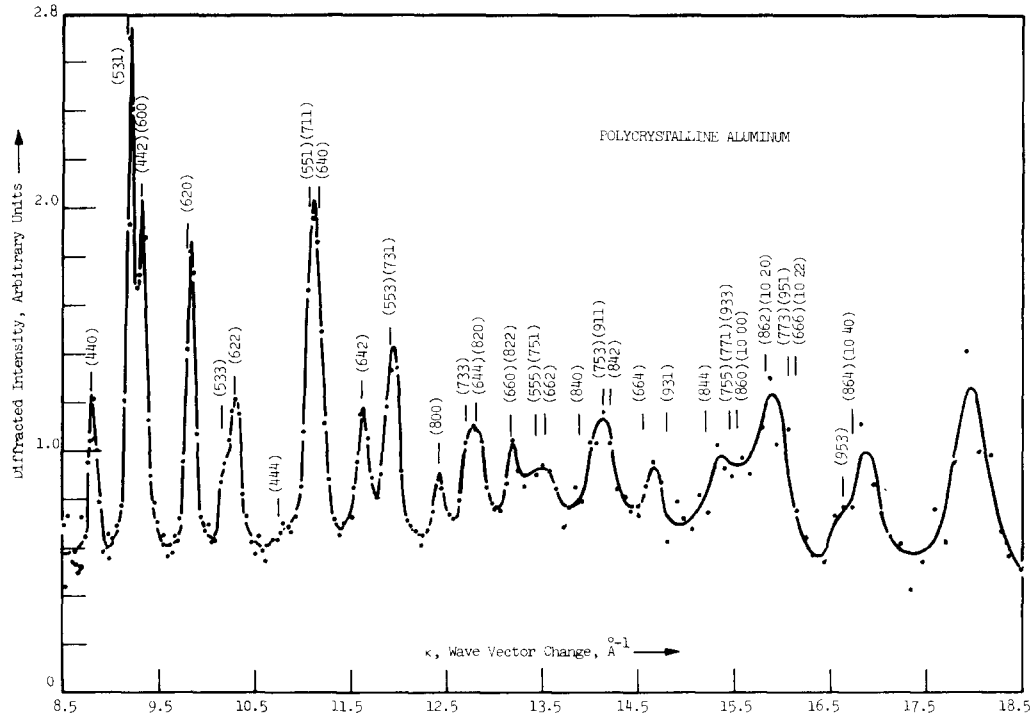

Fig. 6. Neutron diffraction pattern for polycrystalline aluminum.

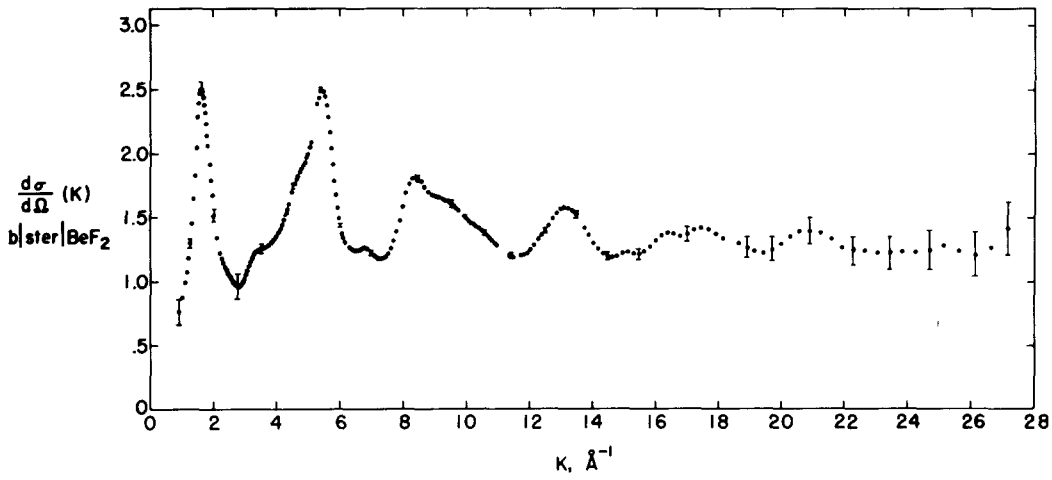

Fig. 7. Neutron diffraction pattern for vitreous BeF_2. Points shown are derived from a cubic splines moothing function fit to the data; error bars represent standard deviation due to statistical error of *individual* points in a region, and not of the spline function itself. Gaps are due to removal of Bragg scattering peaks from the aluminum container.

polycrystalline aluminum and graphite scatterers at various rotor frequencies and at both 20° and 90° scattering angles. Results are shown in fig. 5. As can be seen, the resolution width $\Delta Q/Q$ is less than 2% at all but the highest wave vector transfers at each frequency. Although the resolution at 20° is somewhat larger than at 90°, the actual line broadening at 20° is never more than 0.15 $Å^{-1}$ in the range for which 20° data are used.

To illustrate the resolution characteristics of the instrument, fig. 6 shows the result of a single run with polycrystalline aluminum at 480 Hz and 90°. Wave vector transfers corresponding to several aluminum diffraction lines are indicated. Since this measurement was made in a relatively short time (24 h), statistical imprecision limits the range to somewhat less than 20 $Å^{-1}$.

As an illustration of the power of the instrument, fig. 7 presents the results of a measurement of approximately twelve days duration scattering from a vitreous BeF_2 target. It is again to be emphasized that these long-range data are obtained without application of the severely intensity-reducing measures (e.g. fluorescence excitation or wavelength analysis of the scattered radiation) which must be applied to obtain high quality X-ray data in this wave vector transfer region; and that no Placzek corrections[17]) (which involve energy moments of the scattering law, and in consequence can be calculated only approximately) have been applied to extract the static structure factor from the measured differential cross section. These are presumably minimized in measurements using the equal-flight-path configuration. This has been shown[18]) not to be the case for the calculable first-moment corrections. However, independent detailed inelastic scattering measurements on BeF_2 glass have been integrated to provide the exact static structure factor, and agreement with equal-flight-path structure factor measurements is within the combined (roughly 2%) statistical error of the two measurements[19]).

10. Conclusion

We have described a high-resolution, wide-range TOF neutron diffractometer whose performance is suited to the study of liquids and glasses. Analysis techniques developed to process data from this spectrometer will be described in detail in a separate paper.

References

1) F. Zernicke and J. Prins, Z. Phys. **41** (1927) 184.
2) J. M. Carpenter and J. D. Sutton, Nucl. Instr. and Meth. **99** (1972) 453.
3) J. M. Carpenter, Nucl. Instr. and Meth. **47** (1967) 179; see also A. Holas, report INR-742 (Warsaw, 1966).
4) J. B. Bullock, E. A. Daniels and J. S. King, Trans. Amer. Nucl. Soc. **8** (1965) 302.
5) J. R. Pickles and R. Hazlewood, Harwell report AERE X/PR/2357 (Final 1961).
6) R. Stedman, Chalk River report CRRP-931 (1961).
7) L. A. Wraight, D. H. C. Harris and P. A. Egelstaff, Nucl. Instr. and Meth. **33** (1965) 181.
8) K. F. Graham, University of Michigan Thesis (1971); available from University Microfilms, Ann Arbor, Michigan, U.S.A.
9) N. A. Lurie, Nuclear Engineering Department internal report (1966), unpublished.
10) USAEC document BNL-325, 2nd edition (1958).
11) J. R. Beyster, private communication to J. D. Sutton (1967).
12) D. I. Page, Proc. Phys. Soc. **91** (1967) 76.
13) B. E. Warren and G. Mavel, Rev. Sci. Instr. **36** (1965) 196.
14) P. A. Egelstaff, S. J. Cocking and T. K. Alexander, Chalk River Report CRRP-1078 (1960).
15) R. S. Stone and R. E. Slovacek, USAEC document KAPL-1499 (1956).
16) J. M. Carpenter, University of Michigan Thesis (1963).
17) G. Placzek, Phys. Rev. **86** (1952) 377; see also J. E. Enderby, *Physics of simple liquids*, ed. H. V. N. Temperley, J. S. Rowlinson and G. S. Rushbrooke (North-Holland Publ. Co., Amsterdam, 1968) chapter 14.
18) J. G. Powles, Mol. Phys., to be published.
19) C. A. Pelizzari, University of Michigan Thesis (1973).